CORA Cork Open Research Archive
Cartlann Taighde Oscailte Chorcaí

Title	Improved robustness of ex-situ biological methanation for electro-fuel production through the addition of graphene
Authors	Wu, Benteng;Lin, Richen;Kang, Xihui;Deng, Chen;Dobson, Alan D. W.;Murphy, Jerry D.
Publication date	2021-12-01
Original Citation	Wu, B., Lin, R., Kang, X., Deng, C., Dobson, A. D. W. and Murphy, J. D. (2021) 'Improved robustness of ex-situ biological methanation for electro-fuel production through the addition of graphene', Renewable & Sustainable Energy Reviews, 152, 111690 (13pp). doi: 10.1016/j.rser.2021.111690
Type of publication	Article (peer-reviewed)
Link to publisher's version	10.1016/j.rser.2021.111690
Rights	© 2021 The Author(s). Published by Elsevier Ltd. This is an open access article under the CC BY license (http://creativecommons.org/licenses/by/4.0/) - https://creativecommons.org/licenses/by/4.0/
Download date	2026-11-05 23:23:05
Item downloaded from	https://hdl.handle.net/10468/13400

UCC
University College Cork, Ireland
Coláiste na hOllscoile Corcaigh

Renewable and Sustainable Energy Reviews 152 (2021) 111690

Contents lists available at ScienceDirect

Renewable and Sustainable Energy Reviews

journal homepage: www.elsevier.com/locate/rser

Improved robustness of *ex-situ* biological methanation for electro-fuel production through the addition of graphene

Benteng Wu [a,b], Richen Lin [a,b,*], Xihui Kang [a,b], Chen Deng [a,b], Alan D.W. Dobson [a,c], Jerry D. Murphy [a,b,**]

[a] MaREI Centre, Environmental Research Institute, University College Cork, Cork, T23 XE10, Ireland
[b] Civil, Structural and Environmental Engineering, School of Engineering and Architecture, University College Cork, Cork, T12 YN60, Ireland
[c] School of Microbiology, University College Cork, Cork, T12 K8AF, Ireland

ARTICLE INFO

Keywords:
Ex-situ biomethanation
Carbonaceous materials
Intermittent gas supply
Power to gas
Syntrophic acetate oxidation

ABSTRACT

Ex-situ biomethanation ($CO_2 + 4H_2 \rightarrow CH_4 + 2H_2O$) can simultaneously achieve renewable electricity storage and CO_2 valorisation. However, fluctuations in variable renewable electricity may lead to intermittent hydrogen supply, which is shown to adversely affect microbial activity and performance of the biomethanation process. Carbonaceous materials may act as an abiotic additive to enhance microbial robustness and improve system performance. Nanomaterial graphene and pyrochar were compared to assess their effects on biomethanation systems with an intermittent supply of hydrogen. Results revealed that intermittent gas supply caused deterioration in the restart performance with only 66% of theoretical methane production obtained in the control compared with 84% under steady state conditions. The addition of graphene in biomethanation led to 78% of the theoretical methane production after repetitive intermittent supply; this improvement is postulated to be due to its high electrical conductivity and large specific surface (500 m^2/g). In comparison, pyrochar amendment did not lead to a significant improvement in upgrading performance. Microbial analysis showed that the OTUs affiliated to bacteria withinin the order *SHA-98* (42.9% in abundance) and archaea from the genus *Methanothermobacter* (99%) may result in the establishment of a new syntrophic relationship to improve the robustness of biomethanation process.

1. Introduction

The increasing resource of variable renewable electricity, such as from wind farms and photovoltaic arrays, has played and will continue to play an increasingly important role in reducing greenhouse gas emissions [1]. However, the intermittent nature of variable renewable electricity has highlighted the challenge in efficient energy storage and utilization of existing infrastructure [2,3]. It is highly likely that the private transportation sector will be predominately electrified in the near future, but this is less likely and in some cases improbable for heavy-duty transport such as planes, ships, and long-haul trucks [4,5]. The alternative to direct electrification of transport includes for increasing levels of hydrocarbon fuel production *via* CO_2 reduction [1]. In essence indirect electrification using power to gas (P2G) technologies to produce electro-fuels can enable storage of variable renewable electricity whilst reducing levels of electricity curtailment. The first step in power to gas is electrolysis to produce hydrogen; secondary steps present opportunities to react hydrogen with CO_2 (sourced from preferable biogenic sources such as the CO_2 in biogas) to produce infrastructure-compatible transportation fuels such as methane. The methanation of CO_2 can be conducted thermochemically or biologically [6]. Thermochemical or catalytic Sabatier systems involve high temperature and pressure systems employing catalysts which require prior cleaning of the biogas to remove contaminants [7]. Biological methanation (biomethanation, also known as hydrogenotrophic methanogenesis) is capable of producing high quality methane under mild conditions without using metal catalysts or the requirement for a pre-cleaning step [8,9].

Generally, biological methanation can be classified into two categories or configurations: *in-situ* within the anaerobic digester or *ex-situ* in a separate reactor with isolated hydrogenotrophic methanogens [10,11]. *In-situ* biomethanation can lead to the accumulation of volatile fatty acids (VFAs) due to the increased hydrogen partial pressure associated

* Corresponding author. MaREI Centre, Environmental Research Institute, University College Cork, Cork, T23 XE10, Ireland.
** Corresponding author. MaREI Centre, Environmental Research Institute, University College Cork, Cork, T23 XE10, Ireland.
E-mail addresses: richen.lin@ucc.ie (R. Lin), jerry.murphy@ucc.ie (J.D. Murphy).

https://doi.org/10.1016/j.rser.2021.111690
Received 29 April 2021; Received in revised form 11 August 2021; Accepted 10 September 2021
Available online 20 September 2021
1364-0321/© 2021 The Authors. Published by Elsevier Ltd. This is an open access article under the CC BY license (http://creativecommons.org/licenses/by/4.0/).

Nomenclature

AD	Anaerobic digestion
DIET	Direct interspecies electron transfer
MIET	Mediated interspecies electron transfer
OTUs	Operational taxonomic units
P2G	Power to gas
SAO	Syntrophic acetate oxidation
VFAs	Volatile fatty acids

with a reduction in the favourability of acetogenesis and elevated pH resulting from bicarbonate consumption; this is not an issue for *ex-situ* systems since the process takes place in a vessel which is separate from the original anaerobic digestion (AD) process [12]. Several studies have shown that *ex-situ* biomethanation can accept higher hydrogen loading rates and obtain higher gas conversion rates when compared with the *in-situ* strategy [13–15].

The P2G system connects electrical and gas infrastructure and ideally optimises existing energy infrastructure. McDonagh et al. [16] investigated the relationship between the electricity market and the production of electro-fuels showing that for economic production the electrolyser could not depend on just curtailed electricity but needed to operate ideally in excess of 6000 h per year. Intermittency in hydrogen availability was shown to be associated with seasonal and demand variations [2,6]. This adds a technical challenge to the optimal operation of a biomethanation system. Increasing deterioration of the biomethanation process was found for restart periods with increasing repetitions of intermittent gas injection; Strübing et al. [2] showed that for standby periods of 2 d the methane production rate reduced by 9.9%. Similar observations were also reported by Logroño et al. [6] who found that a 7 d standby period resulted in a significant reduction in restart methane production rates, which decreased by between 5.6 and 18.8% depending on the inoculum. Effective strategies are therefore needed to minimize the adverse impact on biomethanation performance due to intermittent gas supply.

In recent studies, the amendment of carbonaceous materials such as pyrochar and activated carbon has been suggested as an approach to enhance the stability and performance of AD [17–19]. Benefits from the application of carbon-based nano-catalysts such as graphene in the AD domain have also been highlighted [20]; their unique properties including morphologic variety, chemical stability and large surface area are suggested to facilitate the biomethane yield or production rate during AD [21]. Nanomaterial graphene addition was shown to improve the stability of digesters and accelerate the recovery of the methanogenesis function after experiencing external stress (for example acidic shock) possibly due to accelerated direct interspecies electron transfer (DIET) [4]. Similar mitigatory effects were also found when pyrochar was added to alleviate the stress of ammonia and acid inhibition during AD; the immobilization effect of pyrochar on functional microbes was highlighted [22]. To the best of the authors' knowledge, the addition of carbonaceous materials in biological methanation systems has not to date been studied with the exception of Yang et al. [23] who used pyrochar to enhance the methane production rate during *ex-situ* biogas upgrading. The large specific surface area and functional groups of pyrochar were assumed to be the main contribution to the improved methane production rate of over 70% [23]. However, despite this there is a gap in the state of the art in the potential role of carbonaceous materials in *ex-situ* biomethanation systems facing flexible operation conditions due to intermittent gas injection.

The innovation in this work is that it is the first assessment of the potential role of carbonaceous materials in *ex-situ* biomethanation systems operating with a variation in gas supply. To realise the innovation the paper has the following objectives:

- Evaluate the application of carbonaceous materials in an *ex-situ* biomethanation system with a particular focus on their effect on biomethanation efficiency and evolution of the microbial community structure with an intermittent gas supply.
- Assess differentiation in operation using nanomaterial graphene and the more cost-effective pyrochar operating under batch mode.
- Investigate process parameters that impact on gas conversion efficiency including for variations in VFA concentration and composition, hydrogen mass balance and pH change.
- Undertake microbial community profiles analysis for different operational periods including steady state and intermittent gas injection period.
- Provide evidence of optimal potential functional microbes for *ex-situ* biomethanation biogas upgrading.

2. Materials and methods

2.1. Inoculum and material

The inoculum for *ex-situ* biomethanation start-up was originally obtained from a lab-scale thermophilic (55 ± 1 °C) reactor treating a wide range of feedstocks including cattle manure, thin stillage (sourced from a local whiskey distillery in Ireland [17]), and seaweed. Prior to the biomethanation experiments, the inoculum was sieved over a 600 μm mesh to remove undigested large particles and then fed with a H_2 and CO_2 gas mixture (volume ratio of 4:1) for several cycles to enrich the hydrogenotrophic methanogens. The main properties of the inoculum are listed in Table 1.

Pyrochar was produced from pyrolysis of waste wood at 700 °C with a practical size of less than 150 μm after grinding and sieving. Graphene nanosheets were purchased from Sigma-Aldrich with a length of less than 2 μm. Their detailed properties were shown in a previous study [17].

2.2. System configuration and operation

The *ex-situ* biomethanation systems include the glass bottle, gas bag and peristaltic pump (Fig. S1). Serum bottles (working volume of 400 mL) were used as the reactor, which contained 206 mL of inoculum and 194 mL of basal medium, leading to a concentration of volatile solids of 10 g/L. The basal medium contained the necessary nutrients for the growth and metabolism of microorganisms. The compositions per litre of basal medium are as follows: 750 mg KH_2PO_4, 1450 mg $K_2HPO_4{\cdot}3H_2O$, 900 mg NH_4Cl, 168 mg $MgCl_2$, 10 mL trace element solution and 10 mL vitamin solution. The trace element solution consisted of (in 1 L stock solution): 10 mg $MnCl_2$, 50 mg $ZnCl_2$, 10 mg H_3BO_3, 10 mg $CaCl_2$, 10 mg Na_2MoO_4, 200 mg $CoCl_2{\cdot}6H_2O$, 10 mg $AlK(SO_4)_2$ and 10 mg $NiCl_2{\cdot}6H_2O$. The vitamin solution contained (in 1 L stock solution): 100 mg glutamic acid, 25 mg ascorbic acid, 25 mg riboflavin, 20 mg citric acid monohydrate, 10 mg folic acid, 10 mg 4-aminobenzoic acid and 25 mg creatine. Gas bags (volume capacity

Table 1
Main characteristics of inoculum.[a]

Parameters	Inoculum
Total solids (g/L)	31.87 ± 0.42
Volatile solids (g/L)	19.40 ± 0.20
pH	8.11
Total nitrogen (mg/L)	2953 ± 103
Ammonia nitrogen (mg/L)	2376 ± 70
Acetate (mg/L)	410
Propionate (mg/L)	276
Isobutyrate (mg/L)	57
Isovalerate (mg/L)	9

[a] The average value and standard deviation are based on triplicate tests.

1000 mL) were used to store the gas mixture and balance the overall system pressure during upgrading. A peristaltic pump was adopted to circulate the gas in the experimental set up at 27 rpm, giving a calibrated gas flow rate of 33.7 ± 0.8 mL/min (based on 9 repetitions). The pressure of the pump was 1 atm.

To investigate the influence of carbonaceous materials on the performance of the *ex-situ* biomethanation process, a control group (without addition of conductive materials), graphene group (1.0 g graphene/L) and pyrochar group (1.0 g pyrochar/L) were adopted with corresponding materials introduced into different series of bottles. One of our previous studies highlighted that 1.0 g graphene/L could stabilize the AD process after encountering an acidic shock [17]. The same dosage of pyrochar and graphene (1.0 g/L) was chosen to compare their potential influence on this biomethanation system which also undergoes stress. Due to the channel limitation of the pump (8 channels in total), the control group was conducted in duplicate, which required 2 channels, while the graphene and pyrochar group were performed in triplicate, which required 6 channels. The pH in each reactor was initially adjusted to 8.11 ± 0.01 with HCl (6 M) and NaOH (6 M). After purging with nitrogen (99.998% in purity) for 2 min, gases in the 200 mL headspace of the reactors were replaced by the H_2 (99.999% in purity) and CO_2 (99.8% in purity) gas mixture (volume ratio of 4:1). Afterwards, tygon tubing (ACF00006-C, Masterflex, Germany) was used to connect the gas bag, reactor, and circulation pump; tygon tubing was used due to its low gas permeability. The inner diameter of tubing was 2.79 mm and the total length used was approximately 1.5 m per reactor. The experiments were conducted in a constant temperature shaking incubator at 55 ± 1 °C and 300 rpm. The biomethanation experiments were carried out for 9 cycles (each with a gas retention time of 24 h). After each cycle, the entire system was flushed with the H_2 and CO_2 gas mixture, re-achieving a total working volume of 1200 mL at room temperature (namely 200 mL in the reactor headspace and 1000 mL in the gas bag). It should be noted that the gas volume within the connecting tubing (approximately 9.2 mL per reactor) was not considered in the total working volume. To study the potential effect of intermittent gas injection on the performance of *ex-situ* biomethanation systems, cycle 4 and 6 were restarted after a standby period of 2 d and 1 d, respectively. This was the stress imposed on the system. Detailed operational parameters including the gas retention time, feeding gas concentration, gas loading rate are highlighted later in Table 2 in the Results section.

2.3. Analytical methods

The total solids and volatile solids were measured in triplicate according to methods outlined in a previous study [24]. The volume of output gas in the gas bags was measured with a syringe, a 3-way stopcock and an empty gas bag (Fig. S2). Detailed operations of gas volume measurement are described in the supporting information. The output gas volume was determined as the sum of the gas volume in the gas bag and the reactor headspace. The output gas volume presented in this study was normalized to the standard conditions (273.15 K, 1 atm). The gas composition (CO_2, H_2 and CH_4) and VFA contents (acetic acid, propionic acid, isobutyric acid, isovaleric acid, isocaproic acid and caproic acid) in the liquid effluents were determined by gas chromatography (Agilent 7890B, USA); equipment configuration and corresponding analysing methods are detailed in the supporting information. pH data was collected by an F20 pH meter (METTLER TOLEDO, Switzerland). Total nitrogen and ammonia nitrogen were quantified in triplicate using total nitrogen reagent kits (LCK 238, Hach, USA) and ammonia reagent kits (2606945, Hach, USA), respectively, with a spectrophotometer (DR3900, Hach, USA). The electrical conductivity of the suspended sludge was determined as described by Zhao et al. [25] with minor modifications. Briefly, 30 mL of the suspended sludge was collected from each reactor at the end of the experiment. After washing with 0.9% NaCl solution (30 mL) *via* centrifugation at 5300 rpm for 5 min three times, the sludge pellet was placed on two-gold electrodes across a non-conductive gap (25 mm × 0.5 mm × 0.1 mm). An electrochemical workstation (Biologic VSP, France) was adopted to apply a voltage increasing from −0.3 V to 0.3 V with a voltage ramp of 25 mV/s. The time average current of each applied voltage was recorded to establish the current–voltage curve, the slope of which was used to calculate the electrical conductivity. Parameter values for the control group were presented based on duplicate tests, while for the graphene and pyrochar group were based on triplicate tests.

Table 2
Design and performance characteristics of *ex-situ* biomethanation systems.

Parameter	Control	Graphene	Pyrochar
Dosage (g/L)	0	1.0	1.0
Gas retention time (h)	24	24	24
H_2 injection (%)	80.2 ± 0.75	80.2 ± 0.75	80.2 ± 0.75
CO_2 injection (%)	19.8 ± 0.75	19.8 ± 0.75	19.8 ± 0.75
H_2 loading ($L/L_{VR}/d$)[a]	2.24 ± 0.02	2.24 ± 0.02	2.24 ± 0.02
CO_2 loading ($L/L_{VR}/d$)	0.55 ± 0.02	0.55 ± 0.02	0.55 ± 0.02
CH_4 output ($L/L_{VR}/d$)			
Steady state[b]	0.47 ± 0.03	0.46 ± 0.03	0.45 ± 0.02
Cycle 4	0.47 ± 0.003	0.46 ± 0.02	0.46 ± 0.002
Cycle 6	0.37 ± 0.12	0.44 ± 0.002	0.069 ± 0.018
H_2 output ($L/L_{VR}/d$)			
Steady state[b]	0.002 ± 0.005	0.007 ± 0.012	0.004 ± 0.007
Cycle 4	0.00 ± 0.00	0.00 ± 0.00	0.00 ± 0.00
Cycle 6	0.40 ± 0.56	0.00 ± 0.00	1.76 ± 0.06
CO_2 output ($L/L_{VR}/d$)			
Steady state[b]	0.037 ± 0.008	0.036 ± 0.009	0.036 ± 0.007
Cycle 4	0.036 ± 0.005	0.035 ± 0.003	0.034 ± 0.002
Cycle 6	0.061 ± 0.044	0.031 ± 0.002	0.21 ± 0.02
Gas conversion efficiency (%)			
Steady state[b]	83.87 ± 4.96	82.56 ± 5.81	80.95 ± 3.85
Cycle 4	84.02 ± 0.61	82.47 ± 3.83	81.20 ± 0.42
Cycle 6	65.77 ± 21.53	77.72 ± 0.33	12.37 ± 3.26

[a] VR means the working volume of the reactor (400 mL); values are the average of cycle 1 to cycle 9.
[b] Values are calculated from the average of cycle 2, 3, 8, and 9; cycle 4 was restarted after intermittent gas injection for 2 d; cycle 6 was restarted after intermittent gas injection for 1 d.

2.4. Microbial community analysis

To investigate the microbial community structure in the three groups, seven liquid samples (4 mL per sample) were collected using a syringe during the upgrading experiments; one was obtained from the inoculum whilst the remaining six samples were obtained from the control group (cycle 6 and 9), graphene group (cycle 6 and 9) and pyrochar group (cycle 6 and 9). The samples were stored at −20 °C before DNA extraction and further analysis. For bacterial 16S rRNA gene amplification of DNA extracts, primers 338F/806R were selected to target the V3–V4 hypervariable regions. For archaeal 16S rRNA gene amplification of DNA extracts, primers 524F10extF/Arch958RmodR were chosen to target the V4 hypervariable regions. Polymerase chain reaction product processing, Illumina sequencing, and data analysis were performed as reported previously [17]. Taxonomic classification of each sequence was characterized by RDP Classifier 2.11 (https://sourceforge.net/projects/rdp-classifier/) against the Greengene database Release 13.5 (http://greengenes.secondgenome.com/). The raw sequence data was deposited into the Sequence Read Archive of NCBI under a BioProject accession code PRJNA723741.

2.5. Calculations

2.5.1. Electrical conductivity (μS/cm)

The electrical conductivity of the sludge was calculated based on Eq. (1):

$$\sigma = \frac{L}{R \times S} \quad (1)$$

where σ (μS/cm) is the electrical conductivity, L (cm) is the width of the non-conductive gap (0.05 cm), R (μS) is the reciprocal value of the slope of the current–voltage curve, and S (cm^2) is the cross-sectional area of the non-conductive gap (0.025 cm^2).

2.5.2. Normalization of gas volume (mL)

The gas volume was normalized according to Eq. (2).

$$V_{gas} = \frac{V \times T_s}{T} \quad (2)$$

where V_{gas} (mL) is the gas volume under standard conditions (273.15 K, 1 atm), V (mL) is the measured gas volume, T_s (K) is the standard temperature (273.15 K), and T (K) is the room temperature, assuming at 293.15 K. The system pressure was assumed to be 1 atm during upgrading. Pressure disturbance caused by the peristaltic pump and water content in the gas mixture caused by water vapor were not considered in the calculation.

2.5.3. Gas loading rate ($L/L_{VR}/d$)

The loading rate of H_2 or CO_2 was calculated based on Eq. (3).

$$Gas\ loading\ rate = \frac{V_{gas-in}}{V_{reactor} \times t} \quad (3)$$

where $V_{gas\text{-}in}$ (L) is the gas loading volume under standard conditions (273.15 K, 1 atm), $V_{reactor}$ (L_{VR}) is the working volume of reactor (0.4 L_{VR}), and t (d) is the gas retention time (1 d).

2.5.4. Gas output ($L/L_{VR}/d$)

The output of H_2, CO_2 and CH_4 was calculated based on Eq. (4).

$$Gas\ output = \frac{V_{gas-output}}{V_{reactor} \times t} \quad (4)$$

where $V_{gas\text{-}output}$ (L) is the gas output volume under standard conditions (273.15 K, 1 atm), $V_{reactor}$ (L_{VR}) is the working volume of reactor (0.4 L_{VR}), and t (d) is the gas retention time (1 d)."

2.5.5. Gas conversion efficiency (%)

The success of H_2 and CO_2 forming CH_4 is defined by the conversion efficiency, which is calculated according to Eq. (5).

$$Gas\ \text{conversion}\ \ \text{efficiency} = \frac{V_{CH_4}}{V_{theory}} \quad (5)$$

where V_{CH4} (mL) is the CH_4 yield and V_{theory} (mL) is the theoretical CH_4 production (224 mL) based on the Sabatier reaction: $4H_2$ (895 mL) + CO_2 (224 mL) → CH_4 (224 mL) + $2H_2O$; the gas volume shown is under standard conditions.

2.5.6. H_2 balance

In an *ex-situ* biomethanation system, hydrogen is generally utilized *via* two pathways, namely hydrogenotrophic methanogenesis ($4H_2 + CO_2 \rightarrow CH_4 + 2H_2O$) and homoacetogenesis ($4H_2 + 2CO_2 \rightarrow CH_3COOH + 2H_2O$). The produced acetate can further be consumed by acetoclastic methanogens to produce methane and carbon dioxide ($CH_3COOH \rightarrow CH_4 + CO_2$). H_2 equivalents in the form of acetate is calculated according to the following stoichiometry (Eq. (6)):

$$N_{H_2,\,Ac} = C_{Ac} \times V_{reactor} \times 4 \quad (6)$$

where $N_{H2,Ac}$ (mmol) is the amount of H_2 equivalents existing as acetate, C_{Ac} (mmol/L) is the molar concentration of acetate in the effluent, and $V_{reactor}$ (L_{VR}) is the working volume of the reactor.

H_2 equivalents in the form of CH_4 was calculated as Eq. (7):

$$N_{H_2,\,CH_4} = \frac{V_{CH_4} \times 4}{22.4} \quad (7)$$

where $N_{H2,CH4}$ (mmol) is the amount of H_2 equivalents existing as CH_4, and V_{CH4} (mL) is the CH_4 production.

2.5.7. Statistical analysis

Significance analysis of the experimental data was carried out using the one-way analysis of variance (ANOVA) at a p-level of 0.05. The analysis was performed using the software Origin 8.5 (USA).

3. Results and discussion

3.1. Performance of ex-situ biomethanation systems with intermittent gas supply

3.1.1. Control group

The biomethane yield and output gas contents at the end of each cycle are illustrated in Fig. 1. For the control group without graphene or pyrochar addition, the inoculum exhibited an excellent capacity to convert H_2 and CO_2 into CH_4 at the initial phase, resulting in a biomethane production of 186 mL in cycle 1 (Fig. 1A); this is 82.9% of the theoretical yield (224 mL). With continuous gas injection, the biomethane yield increased slightly to 85.4% and 89.7% of the theoretical yield in cycle 2 and 3, respectively. This could be explained by the microbial acclimation effect which has also been observed in other studies [6,14]. The first intermittent gas injection was enforced in cycle 4 with a break in operation for 2 d. However, it did not lead to a significant influence on biomethane production. The biomethane yield in cycle 4 only decreased to 84.0% of the theoretical yield compared with 89.7% for cycle 3. After the operation of one cycle, biomethane production in cycle 5 recovered to 197 mL, 88.1% of the theoretical yield. However, a clear impairment in upgrading performance was observed after the second break in operation for one day before cycle 6, leading to a biomethane production of 147 mL, 65.8% of the theoretical yield.

The portion of methane in the output gas (Fig. 1B) increased from 88.6% to 95.1% from cycle 1 to cycle 5 with CO_2 as the dominant residual. In cycle 6 after a one-day break in operation it significantly decreased to 58.4% with H_2 as the main residual (Fig. 1B); this reinforces the deterioration of gas conversion led by the repetitive intermittent gas injection. Similar findings were reported by Strübing et al. [2] who revealed that adverse effects on restart performance were negligible during the first intermittent gas injection (with a standby period of 2 d) whereas subsequent breaks resulted in the hydrogen content of the output gas increasing up to 60%. Tsapekos et al. [26] also reported a serious deterioration in upgrading performance after a longer standby period of 25 d, decreasing the output methane content from 90% to approximately 25%; full recovery of methanogenic activity was achieved after 6 d continuous operation. The inhibitory effect did not last for long in this study since the biomethane yield quickly reached 94.0% of the theoretical production in cycle 7 whilst the methane concentration reached 93.2%; this might be attributed to the shorter standby period compared with other reported studies [2,26]. For cycle 8 and 9, the biomethane yield and content were relatively constant, approximating 180 mL biomethane yield and 93% CH_4 in the output gas, respectively; this indicates that the biomethanation upgrading process returned to stability. The results suggested that repetitive intermittent gas injection could affect the robustness of the biomethanation system, but a recovery can be expected when restoring continuous gas supply.

3.1.2. Carbonaceous material addition

With the addition of carbonaceous materials, the graphene and pyrochar group did not show a significant difference ($p > 0.05$) compared with the control in the initial 4 cycles (including the first intermittent gas injection of 2 d duration), during which the average biomethane production for control, graphene and pyrochar group was 192 ± 7 mL, 187 ± 7 mL and 185 ± 3 mL, respectively, whilst the corresponding average methane content was 90.9 ± 2.0%, 90.8 ± 2.8%

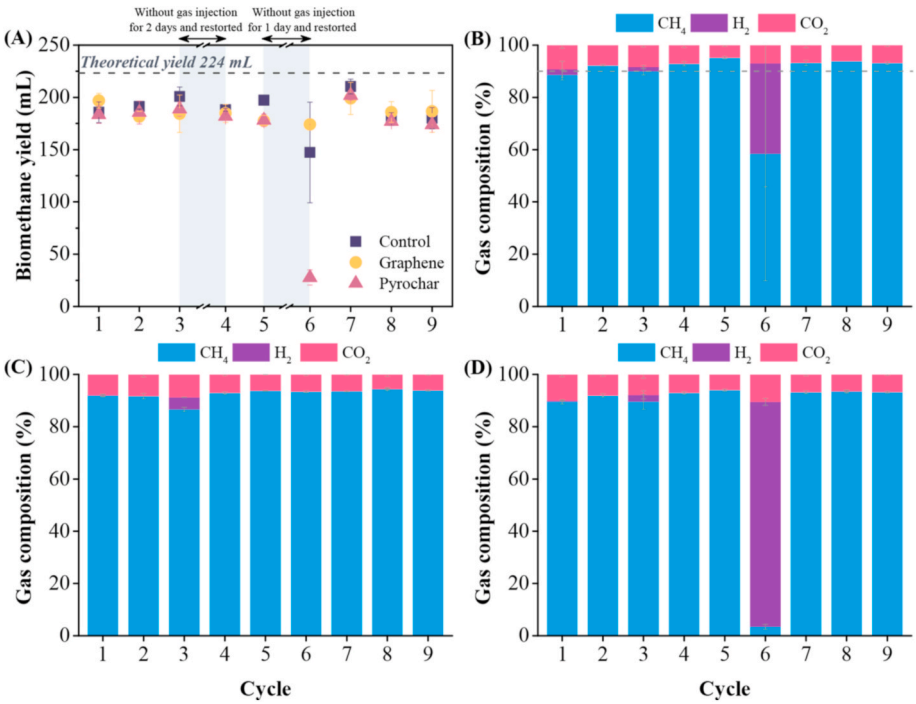


Fig. 1. The biomethane yield (A) and methane, hydrogen and carbon dioxide contents of the control group (B), graphene group (C) and pyrochar group (D) at the end of each cycle. Error bars represent the standard deviation.

and 91.0 ± 1.7%, respectively.

However, the second break in gas injection of a one-day period (cycle 6) led to definite effects being observed on the biomethanation system. For the graphene group, 174 mL of biomethane yield was obtained, 18.2% higher than that of the control. The output gas was dominated with methane, accounting for 93.4% of total gases; 60.0% higher than that of the control. Surprisingly this was not matched by the pyrochar group, where in contrast suppressive effects on the restart performance occurred in this group after the shock of repetitive intermittent gas injection phases, resulting in a significant decline in biomethane yield from 178 mL to 28 mL ($p < 0.05$). This was accompanied by a significant reduction in methane content from 94.0% to 3.4% with hydrogen as the main residual, highlighting that the activity of hydrogenotrophic methanogens was significantly inhibited. We postulate that this may result from the low dosage (1 g/L) and surface area (162 m^2/g) of pyrochar. A detailed discussion can be found in section 3.2.3.

3.1.3. *Comparison of the control group with carbonaceous material addition*

Table 2 outlines the performance characteristics of the *ex-situ* biomethanation trails. Cycle 2, 3, 8 and 9 were chosen as the steady period to compare with cycle 4 and 6 which experienced intermittent gas injection. In the steady state and in the first intermittent gas injection period (cycle 4), no significant difference was observed between different groups in terms of methane output and conversion efficiency ($p > 0.05$); this is consistent with the observations discussed above.

After experiencing the second intermittent gas injection (cycle 6), the methane output of the control group reduced by 21.6% compared with that of the steady state period, whereas this reduction was only 5.9% in the graphene group. The gas conversion efficiency of the graphene group was 18.2% higher than that of the control. Studies on graphene addition in hydrogen-assisted biomethanation process are sparse. Graphene amendment (1 g/L) in AD has been shown to be capable of stabilizing the digestion process when exposed to an external stress of acidic shock; this was likely attributed to the enhanced microbial electron transfer induced by the high electrical conductivity of graphene [17]. Improvement in AD performance in the presence of graphene was also reported by other studies [24,27].

In contrast, the methane output significantly diminished (by 84.7%) in cycle 6 with the addition of pyrochar, resulting in a gas conversion efficiency of 12.4%. Adverse effects associated with pyrochar addition were observed only for *in-situ* biomethanation. Shen et al. [28] and Linville et al. [29] reported the toxicity of pyrochar on biomethane yield at a high dosage, which was ascribed to the release and dissolution of mono- and divalent cations (such as potassium and calcium) under thermophilic conditions. Reduction in biomethane yield and prolongation of lag time induced by pyrochar were also observed in conventional AD, and the non-selective adsorption characteristic of pyrochar was suggested to be the cause of the observed inhibitory effects [30]. Nevertheless, a fast recovery was observed in the pyrochar group with continuous operation in the present study. Compared with the control, no significant difference regarding biomethane production and content was obtained in the subsequent cycles (7, 8 and 9). These results revealed that graphene amendment can stabilize biomethanation systems from the shock of intermittent gas injection, whereas the effect of pyrochar addition was not positive and a transitory inhibition on the recovery of biomethanation efficiency was observed.

3.2. *Dynamic upgrading profile of ex-situ biomethanation systems*

3.2.1. *Dynamic upgrading profile of the steady state*

To further understand the upgrading process, the hourly gas production was measured to develop a dynamic upgrading profile. Fig. 2 illustrates a detailed insight into the 24-h upgrading period of cycle 4, cycle 6 and cycle 9. In the steady state (cycle 9), the initial 8 h was characterised as the rapid upgrading period as more than 88% of biomethane production was achieved in all groups (Fig. 2E). In this period, the methane concentration reached more than 51% following a 71% volume reduction from 1118 mL to less than 323 mL (Fig. 2F). It should be noted that the conversion of hydrogen and carbon dioxide to methane involves a volume reduction reaction ($4H_2 + CO_2 \rightarrow CH_4 + 2H_2O$); an 80% volume reduction can be theoretically achieved according to this reaction. In the next 16 h upgrading period, the methane content reached at least 93% in all groups, with all hydrogen consumed and

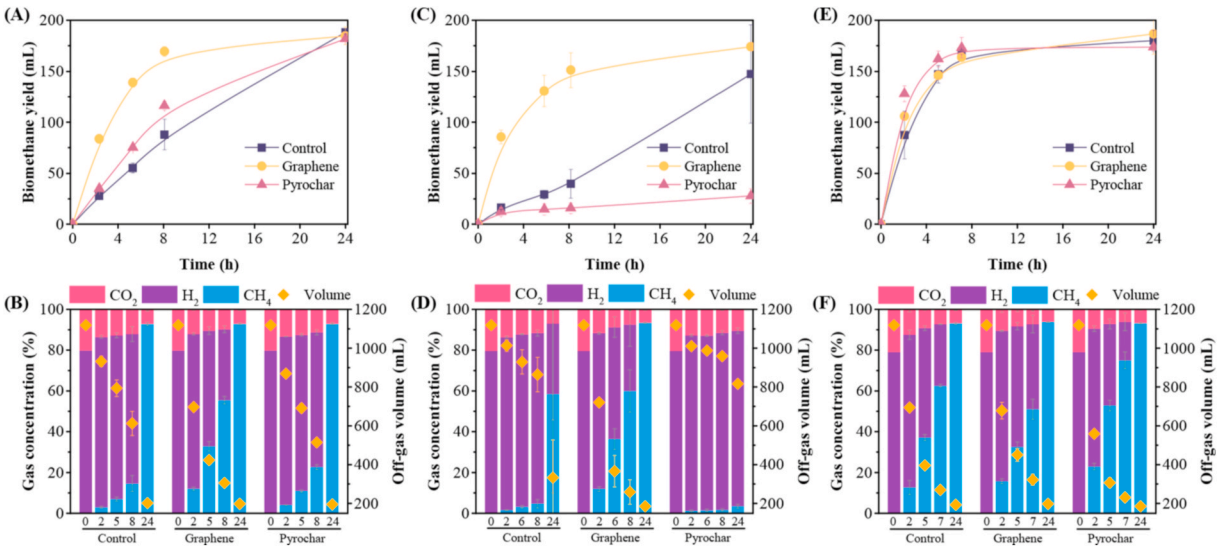


Fig. 2. Dynamic upgrading performance of cycle 4 (A and B), cycle 6 (C and D), and cycle 9 (E and F) (0, 2, 5, 6, 7, 8, and 24 represent the corresponding upgrading hour; cycle 4 was restarted after intermittent gas injection for 2 d; cycle 6 was restarted after intermittent gas injection for 1 d; cycle 9 is selected as the representative steady state cycle). Error bars represent the standard deviation.

approximately 7% carbon dioxide remaining in the off gas. The high carbon dioxide residue could be attributed to hydrolysis of decayed microorganisms [2]. The results revealed that during the steady state, the amendment of carbonaceous materials did not accelerate the upgrading process as no pronounced difference was observed between different groups.

3.2.2. *Dynamic upgrading profile of the intermittent gas injection period*

Comparatively, significant stabilization effects were observed in the graphene group after experiencing the intermittent gas injection (Fig. 2A and C). In cycle 4, graphene amendment accelerated the upgrading efficiency in the initial 8-h period compared to the control. After 8 h of upgrading, the biomethane yield was 169 mL in the graphene group, which is 92.9% higher than that of the control. A relatively lower production of 116 mL was obtained in the pyrochar group, although this figure is still 32.4% higher than that of the control. The off-gas concentration supported this finding: the methane content was 55.5% and 22.6% in the graphene and pyrochar group, respectively, whilst this figure was 14.5% in the control. After 24 h of upgrading, there was no significant difference in the final biomethane yield and methane content among all groups.

The second period of intermittent gas injection (cycle 6) led to a clearer impairment of upgrading performance; the biomethane yield reduced by 55.1% in the control group and by 10.8% in the graphene group compared with that of cycle 4 at hour 8, producing 39 mL and 151 mL, respectively. The most unfavourable system performance was found in the pyrochar group, with only 16 mL methane being produced at hour 8 and 28 mL at hour 24; this is 7% and 12.4% of theoretical yield, respectively.

3.2.3. *Effectiveness of pyrochar*

Yang et al. [23] reported that pyrochar addition can enhance the methane production rate by more than 70% during the *ex-situ* biomethanation process; this was achieved with a pyrochar dosage at 50 g/L (50 times higher addition than in this paper) and continuous gas supply. The large specific surface area (more than 280 m^2/g) and functional groups of pyrochar were highlighted to be beneficial for the immobilization of hydrogenotrophic methanogens [23]. This is supported by the findings from Lü et al. [31] who reported that pyrochar with smaller particle size (<5 μm) at a dosage of 10 g/L aggregated more microbes compared with granular pyrochar due to the significantly improved specific surface area (211 m^2/g), thereby leading to an increase in methane production by 13.3%. In this work, the positive effect was only observed in the first intermittent gas injection while the second starvation resulted in severe impairment on the robustness of the upgrading systems. Considering the much higher specific surface area (500 m^2/g) and the positive effects on restart performance led by graphene, the low dosage (1 g/L) and surface area (162 m^2/g) of the pyrochar used in this study might be ascribed to the poor enhancing effects. However, this assumption cannot be determined with certainty from the results obtained, meaning that further work will be required to investigate the potential correlation between pyrochar dosages, specific surface area and the effect on upgrading performance with repetitive intermittent gas injection.

3.2.4. *Performance over first 8 h*

The biomethane production rate based on the linear fitting of data from the initial 8 h was calculated and is shown in Fig. 3. In cycle 4 (after 2 d of no feeding), the biomethane production rate of the graphene group was 18.9 mL/h, significantly higher than that of the control and pyrochar group (10.4 and 12.1 mL/h, respectively ($p < 0.05$)). Similarly, after the second intermittent gas injection (cycle 6), the biomethane production rate of the graphene group still achieved 16.6 mL/h, whereas this figure for the control and pyrochar group diminished to 4.5 and 1.1 mL/h, respectively. After repetitive intermittent gas injection, the biomethane production rate of the control group significantly decreased from 27.0 (cycle 3) to 10.4 (cycle 4) and finally to 4.5 mL/h (cycle 6). This is supported by findings from Logroño et al. [6] who also observed a significant reduction in biomethane production rates after 7 d and 21 d of starvation under mesophilic conditions. In the steady state cycles (such as cycle 8 and 9), no significant difference was obtained from the biomethane production rate ($p > 0.05$) among all groups, indicating that the addition of graphene delivered a more significant effect on biomethanation recovery subject to intermittent gas supply when compared to biomethanation acceleration in steady state.

T80, which refers to the required time to reach 80% of methane production, is illustrated in Fig. 3B. With the shock of intermittent gas injection, graphene exhibited the best effect in maintaining the biomethane conversion with T80, slightly increasing from 6.5 h in cycle 3 to 7.0 h in cycle 4 and further to 7.7 h in cycle 6. However, for the control group, cycle 4 presented a 220% increase in T80 compared to cycle 3, while cycle 6 presented a 243% increase in T80 compared to cycle 3. The

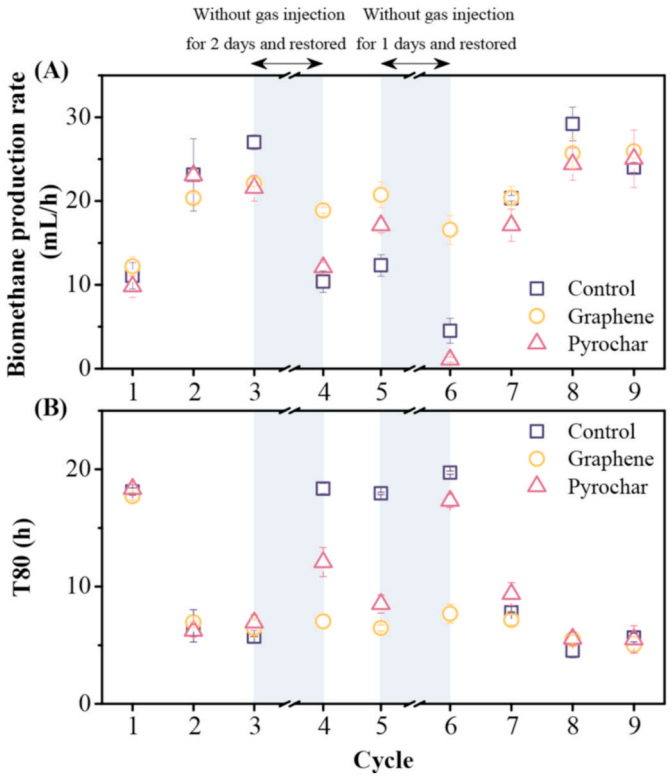


Fig. 3. Variations of biomethane production rate (A) and the required time to reach 80% of the methane yield (B) during upgrading with intermittent gas injection. The biomethane production rate is based on the linear fitting of data from the initial 8 h. Error bars represent the standard deviation.

results of biomethane production rate and T80 in different cycles further support the conclusion that graphene amendment can minimize the shock of intermittent gas supply and stabilize the *ex-situ* biomethanation process, while pyrochar was shown to have a negligible or even negative effect.

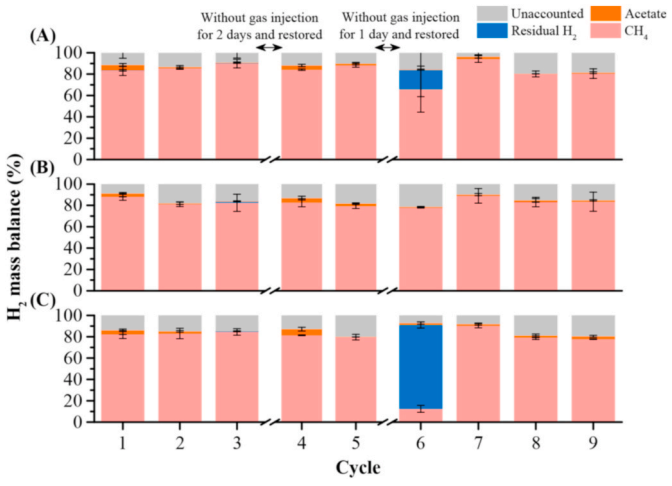


Fig. 4. H_2 mass balance of the control group (A), graphene group (B) and pyrochar group (C) with intermittent gas injection. Error bars represent the standard deviation.

3.3. Hydrogen balance and volatile fatty acids variation during biomethanation

3.3.1. Hydrogen balance

The hydrogen mass balance was analysed to provide insights into the hydrogen conversion pathway during upgrading (Fig. 4). Hydrogen sourced methane is produced *via* either hydrogenotrophic methanogenesis or homoacetogenesis followed by acetoclastic methanogenesis [32]. In the first three cycles, more than 80% of the hydrogen was converted to methane in all groups after the reaction over 24 h whereas the conversion of hydrogen to acetate was negligible, accounting for less than 5% (Fig. 4). Acetate accumulation during the start-up period of biomethanation could be effected by homoacetogenic bacteria and the relatively low activity of acetoclastic methanogens [33]. Conversely, high levels of hydrogen conversion to methane and low acetate accumulation observed in the initial periods tend to indicate the dominance of hydrogenotrophic methanogens in the inoculum; this was confirmed by the microbial profiles in section 3.4.

After experiencing the first intermittent gas injection (cycle 4), the highest accumulation of acetate was obtained in the pyrochar group, accounting for 5.7% of consumed hydrogen, which is 46.6% and 33.4% higher than that of the control and graphene group, respectively. The second intermittent gas injection (cycle 6) did not lead to significant acetate accumulation among the three groups as the conversion of hydrogen to acetate corresponded to less than 1.7% of consumed hydrogen. Throughout the experimental trials, the consumed hydrogen was mainly converted into methane whilst the production of acetate was low in all groups. This indicated that hydrogenotrophic methanogenesis dominated in all reactors. Meanwhile, the unaccounted hydrogen consumption of the control, graphene and pyrochar group was 12.7 ± 4.9%, 15.7 ± 4.4%, and 14.5 ± 4.7% (average of 9 cycles), respectively; this could be ascribed to the loss during sampling and assimilation of biomass [34].

3.3.2. Volatile fatty acids variation

The variation of acetate and propionate concentrations in different cycles is shown in Fig. 5. Due to the minor change through the experimental periods, other VFAs including isobutyric acid, isovaleric acid, isocaproic acid and caproic acid, which together accounted for less than 15% of total amount of VFAs, were not considered as an indicator for the process stability.

From cycle 1 to cycle 3, no significant accumulation of acetate was observed from all groups (Fig. 5A). The average acetate concentration of the control group was 292 ± 23 mg/L, closely followed by the pyrochar group which was 285 ± 18 mg/L and the graphene group which was 259 ± 12 mg/L. However, with the first intermittent gas injection (cycle 4), an apparent increase in the accumulation of acetate was found in all groups, among which the maximum increase of acetate concentration was obtained from the pyrochar group, increasing from 288 to 376 mg/L; this is an increase of 30.3% compared with the prior cycle. The concentration of acetate in the control and graphene groups increased by 20.3% and 24.7%, respectively. Interestingly, the first intermittent gas injection cycle did not lead to a noticeable change in the hydrogen conversion pathway in all groups, as the consumed hydrogen was mainly converted into methane (Fig. 4). Meanwhile, the concentration of propionate which was the second dominant VFA was nearly unchanged in all groups, except for the graphene group, decreasing slightly from 145 to 131 mg/L (Fig. 5B). The results indicated that the accumulated acetate led by the shock of intermittent gas injection may originate from cell decay and subsequent hydrolysis and acidogenesis processes [2]. High levels of VFAs accumulation after intermittent feeding supply has been reported in the AD process. After more than two months of starvation, de Jonge et al. observed a significant increase in acetic acid and propionic acid in thermophilic reactors due to cell decay [35].

After experiencing the second intermittent gas injection (cycle 6), the

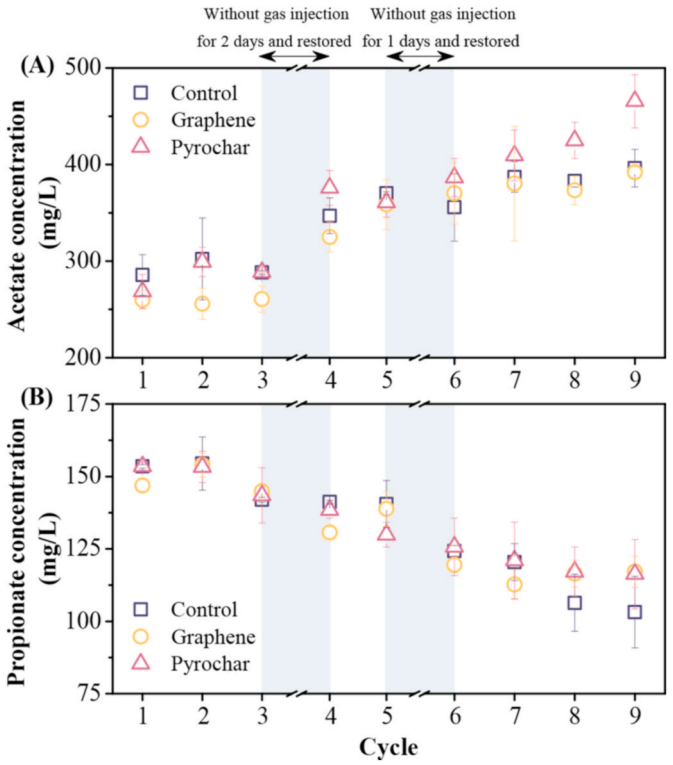


Fig. 5. Variations of acetate (A) and propionate (B) concentrations among different groups at the end of each cycle. Error bars represent the standard deviation.

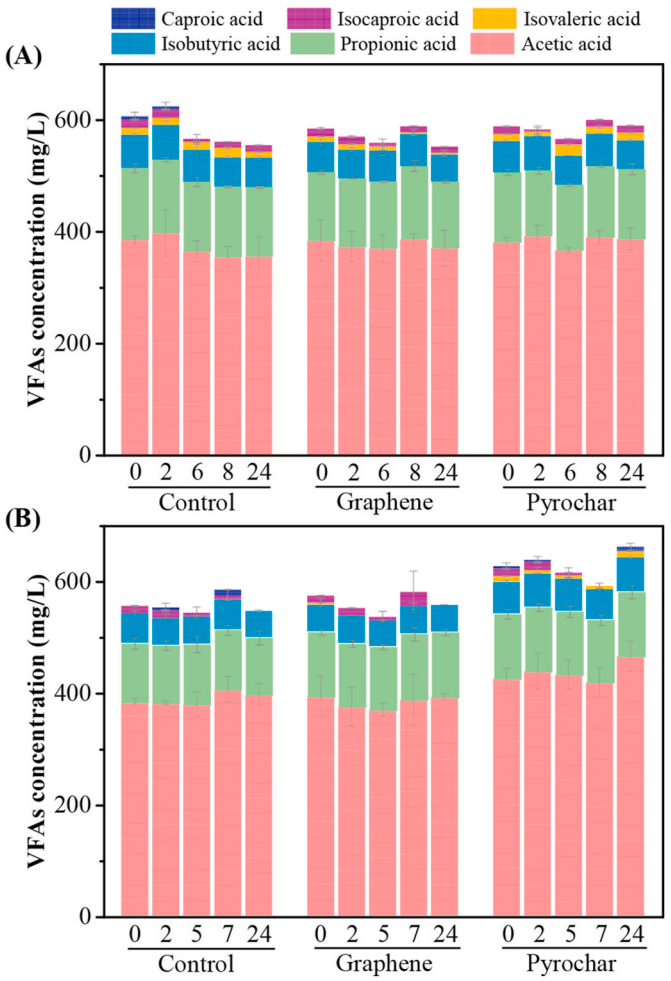


Fig. 6. Volatile fatty acids (VFAs) profile of cycle 6 (A) and cycle 9 (B) in a 24-h upgrading period (0, 2, 5, 6, 7, 8, and 24 represent the corresponding upgrading hour; cycle 6 was restarted after intermittent gas injection for 1 d; cycle 9 was selected to represent the steady state operation). Error bars represent the standard deviation.

most obvious accumulation of acetate was also obtained in the pyrochar group, which increased by 7.2% compared with that of cycle 5. With continuous gas supply, the acetate concentration of the control group increased slightly from 387 to 396 mg/L from cycle 7 to cycle 9. The graphene group also showed similar trends, climbing from 380 to 392 mg/L from cycle 7 to cycle 9. However, a more dramatic acetate accumulation was observed from the pyrochar group during this period, increasing from 409 mg/L in cycle 7 to 465 mg/L in cycle 9: an increase of 13.7%. This rapid increase of acetate concentration in the pyrochar group was accompanied by reduced gas conversion efficiency (Figs. 1A and 4C), decreasing from 90.1% in cycle 7 to 77.6% in cycle 9. This indicated that the accumulated acetate might be produced from hydrogen and carbon dioxide through the homoacetogenesis process.

Throughout the trials, the addition of pyrochar resulted in the most significant accumulation of acetate as 197 mg/L of acetate was obtained from cycle 1 to cycle 9, which is 78.0% higher than that of the control group and 48.9% higher than that of the graphene group. This might result from (1) serious cell decay, leading to acetic acid generation and (2) active homoacetogenesis process ($4H_2 + 2CO_2 \rightarrow CH_3COOH + 2H_2O$) rather than methanogenesis. Another reason could be related to the unbalanced bacterial and archaeal populations in the presence of pyrochar. An optimised cooperation between bacterial and archaeal populations is needed to resist the adverse effects resulting from external stress such as acidic shock and high concentrations of ammonium and acids [17,22,36]. Considering the unaffected gas conversion efficiency in the steady state, it can be assumed that pyrochar addition seems likely to adversely affect the cooperation between bacterial and archaeal populations, thereby weakening the robustness of the *ex-situ* biomethanation systems.

To further explore the hydrogen conversion pathways during upgrading, the VFAs formation of cycle 6 and cycle 9 in a 24-h upgrading period was measured. As can be seen from Fig. 6A, after the shock of repetitive starvation, the total concentration of VFAs varied slightly among all groups. For the control group, the maximum total VFAs concentration was 624 mg/L with acetic acid, and propionic acid dominant, accounting for 63.7% and 21.1%, respectively. After upgrading for 24 h, the total amount of VFAs decreased to 555 mg/L with the composition nearly unchanged. The graphene and pyrochar group showed similar trends in the 24-h upgrading period, during which the concentration of VFAs in the graphene group varied between 552 and 589 mg/L whilst the VFAs in the pyrochar group fluctuated between 566 and 601 mg/L; acetic acid was the dominant VFA in both groups. During the steady state (cycle 9), the total amount of VFAs and the principal VFAs content varied slightly and no significant difference was obtained in all groups (Fig. 6B). Results revealed that intermittent gas injection did not significantly influence the VFAs formation and consumption during biomethanation process. However, the microbial community analysis is required to investigate the potential disturbance and shift in microbial metabolism induced by starvation shock [35,37].

3.4. *Effects of carbonaceous materials on the microbial community during biomethanation*

High-throughput sequencing was used to analyse the 16S rRNA genes of the microbial communities from seven samples, including one inoculum sample and six suspended sludge samples. The six suspended sludge samples were taken from the control group (cycle 6 and 9), graphene group (cycle 6 and 9) and pyrochar group (cycle 6 and 9).

Overall, 942 bacterial OTUs and 21 archaeal OTUs were identified for all samples. Based on these OTUs, 18 genera of bacteria and 1 genus of archaea with a maximum abundance higher than 2% were identified and are displayed in Fig. 7.

3.4.1. Bacterial community during biomethanation

In all groups, most bacteria (63%–84%) belonged to the phylum *Firmicutes*, which is commonly found and reported as the dominant taxa in AD systems [38,39]. The most abundant bacterial populations among all groups were OTUs of the order *MBA08*, order *SHA-98* and family *D2*. Members belonging to *MBA08* and *SHA-98* have previously been revealed to be the dominant bacteria in thermophilic digesters treating food waste, manure, and whiskey by-products [40,41]. The remarkable abundance of OTUs within the order *MBA08* (18.4%) and *SHA-98* (12.9%) in the inoculum highlights their important role in the conventional AD process treating a wide range of carbohydrate-rich feedstocks.

3.4.2. Effects on the bacterial community of intermittent gas injection

After the introduction of H_2 and CO_2, the microbial composition of the inoculum and the carbonaceous materials amended groups exhibited varying levels of change. Compared with the inoculum, a second intermittent gas injection (cycle 6) resulted in a minimum effect on bacterial populations in the control group; the most substantial effect was seen in the graphene group, which is verified by the principal coordinates analysis (Fig. 8). Compared with the inoculum, the microbial compositions of the control group in cycle 6 changed slightly (Fig. 7). The most dominant member was an OTU in the order *MBA08* that decreased from 18.4% to 16.9% whilst the second dominant member, the relative abundance of an OTU in the order *SHA-98* decreased from 12.9% to 10.8% (Fig. 7).

For the graphene group, the most significant modification in the bacterial community structure (in cycle 6) was observed from an OTU in the order *SHA-98*, which increased from 12.9% to 26.2% in relative abundance, and an OTU in the family *D2*, which climbed from 3.9% to 16.7%. Considering that family *D2* belongs to the order *SHA-98*, the relative abundance of *SHA-98*-associated OTUs reached 42.9%, which is significantly higher than that of the control (15.5%) and the inoculum (16.8%), suggesting its potential role in stabilizing the upgrading process and enhancing resilience after experiencing intermittent gas injection. Besides the reported increased tolerance to external pressures such as high concentrations of ammonia [42], members of the order *SHA-98* are also believed to be potentially involved in syntrophic acetate oxidation (SAO) in the biomethanation process [39,43].

Generally, in a biomethanation system, acetate produced from H_2 and CO_2 through the homoacetogenesis process is mainly utilized *via* the acetoclastic methanogenesis process rather than *via* SAO, which aligns with thermodynamic constraints that the energy requirement of converting acetate to H_2 and CO_2 ($\Delta G^{0'} = +94.78$ kJ/mol) is much higher than that of converting acetate to CH_4 ($\Delta G^{0'} = -35.91$ kJ/mol). However, the competitiveness of SAO can be enhanced under certain conditions, such as high ammonia concentrations and hydrogen assisted methanogenesis, in which the activity of acetoclastic methanogens is inhibited [44,45]. Under stressful conditions, community shifts within the microbiota for syntrophic metabolism are a common strategy employed by microbes to resist external impact in the AD system [36,46]. Wintsche et al. [46] observed that a metabolic shift toward SAO coupled with hydrogenotrophic methanogenesis occurred when facing trace element deprivation. Similarly, the working mode for syntrophic metabolism shifting from interspecies hydrogen transfer to DIET was also suggested to resist acidic shock with the assistance of carbonaceous materials [17,36]. The possible roles of bacterial OTUs within the order *SHA-98* in *ex-situ* biomethanation systems have not been previously

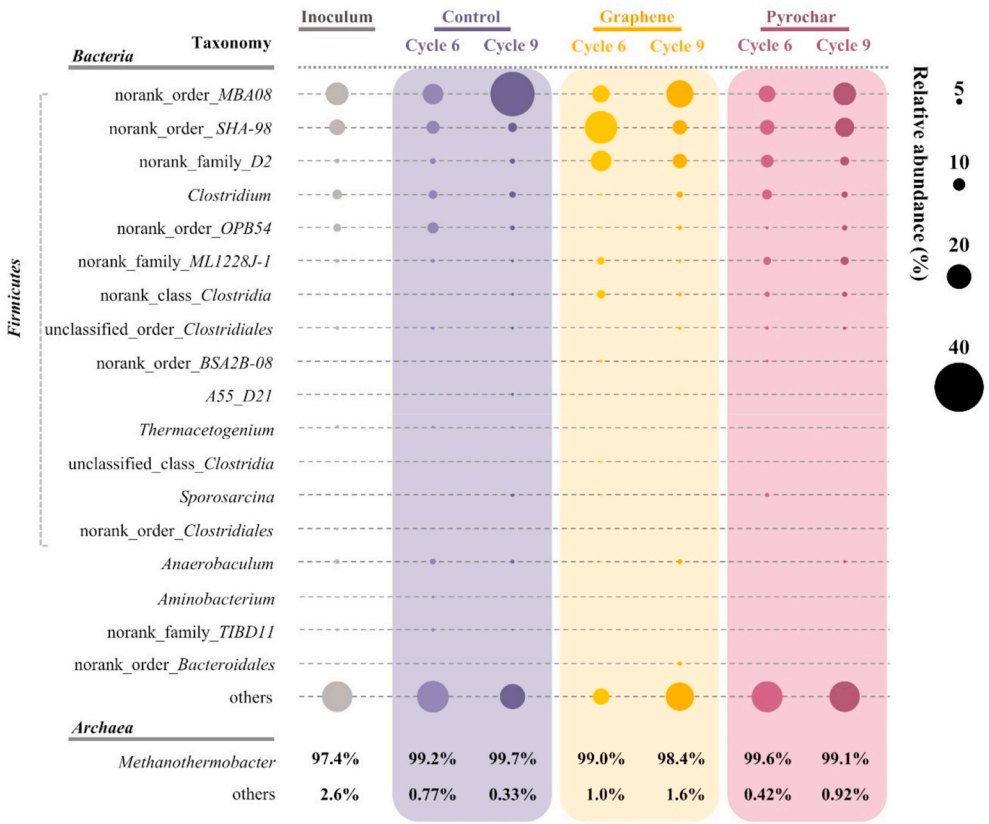


Fig. 7. Microbial community structures at the genus level in different groups. Operational taxonomic units (OTUs) with the relative abundance <2% in all samples are classified into "others" (cycle 6 was restored after intermittent gas injection for 1 d; cycle 9 is selected as the representative steady state). For bacteria, bubble size represents the relative abundance. For archaea, the relative abundance is shown in figures.

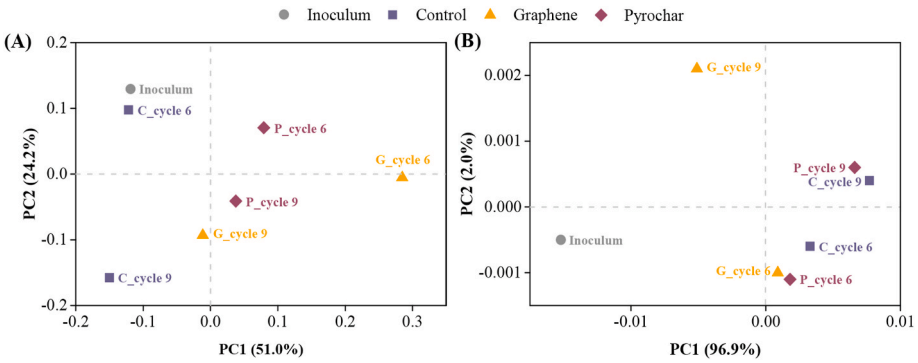


Fig. 8. Principal coordinates analysis of bacteria (A) and archaea (B) on the OTU level (PC: principal component; P: pyrochar group; G: graphene group; C: control group; cycle 6 was restored after intermittent gas injection for 1 d; cycle 9 is selected as the representative steady state).

reported. However, given its predominance over time with graphene amendment under stressful environments (intermittent gas injection in this case) when compared with the control group, it points to a potential critical function for order *SHA-98* in stabilizing the biomethanation system and alleviating external inhibition through SAO with cooperation with hydrogenotrophic methanogens.

3.4.3. Effects on the bacterial community of steady state biomethanation

In steady state (cycle 9), the overall bacterial community structure showed a denser separation pattern among different groups compared with that of cycle 6 (Fig. 8). Similar modifications in OTUs of the order *MBA08* were observed from all groups (Fig. 7), among which the control group showed the most significant modification, increasing from 16.9% (cycle 6) to 36.1% of the total relative abundance, followed by the graphene climbing from 13.9% to 22.0% and pyrochar group increasing from 13.6% to 18.2%. The most apparent deterioration in bacterial composition was observed from the graphene group, in which the relative abundance of OTUs in the order *SHA-98* (including family *D2*) decreased from 42.9% to 22.9%. The predominance of *MBA08* has been reported to indicate the excellent operation of *ex-situ* biomethanation systems possibly through the establishment of syntrophic relationship with hydrogenotrophic methanogens [14,44]. Considering the upgrading performance discussed in section 3.1 and 3.2, the high abundance of an OTU within the order *MBA08* in all groups suggests an essential role in the biomethanation process at steady state.

3.4.4. Effects of carbonaceous materials on the archaeal domain during biomethanation

Regarding the archaeal domain, no obvious separation patterns were observed during the biomethanation process as illustrated in Fig. 8. Compared with the control, the amendment of graphene and pyrochar did not result in marked changes in the archaeal community, and a highly homogenous community was observed throughout the trial. Notably, the most dominant methanogen was common in all groups and exclusively belonged to the genus *Methanothermobacter*, accounting for more than 97% of the total relative abundance (Fig. 7). The predominance of this genus is in accordance with other studies revealing the prevalence and enrichment of hydrogenotrophs within *Methanothermobacter* in thermophilic *ex-situ* biomethanation systems [10,47]. Species belonging to *Methanothermobacter* have been shown to possess unique genes which aid in their survival when they are exposed to various stresses by conferring adaptation to nutritional deprivation and other abiotic stresses [48]. The results indicated that methanogens affiliated with *Methanothermobacter* were selectively enriched over other hydrogenotrophic methanogens and displayed strong resistance to conditions resulting from intermittent gas injection in *ex-situ* biomethanation. Apart from *Methanothermobacter*, *Methanosarcina* mainly accounted for the remaining 2% of abundance. *Methanosarcina* has been reported to function in both acetoclastic and hydrogenotrophic pathways [17,49]. Due to the carbon-limited environment, *ex-situ* biomethanation systems may not be suitable for *Methanosarcina* to employ methanogenesis. Moreover, the low abundance of acetoclastic methanogens in all the groups throughout the experiment suggested that it is unlikely that microbes within the reactor employed a metabolic pathway involving acetoclastic methanogenesis using the acetate produced from the homoacetogenesis process following the shock of intermittent gas injection.

3.4.5. Syntrophic acetate oxidation

Considering the enhanced biomethane yield and production rate after experiencing intermittent gas injection in the graphene group, the significant increase in the relative abundance of possible SAO OTUs within the order *SHA-98* suggest that they may play a critical role in stabilization of the *ex-situ* biomethanation systems, possibly by employing a metabolic pathway involving the SAO processes with the cooperation of the hydrogenotrophic methanogens within the genus *Methanothermobacter*. In the stable state, the predominance of OTUs belonging to the order *MBA08* was found in all groups, indicating its important role in a well-operating *ex-situ* biomethanation system.

3.5. Potential mechanisms responsible for the stabilization effect of graphene on ex-situ biomethanation

Clearly, graphene addition was shown to be capable of stabilizing the biomethanation process after experiencing intermittent gas supply when compared to the control group. Since acetate was the dominant VFA throughout the trials, thermodynamic calculations were conducted to evaluate the Gibbs free energy values of acetate conversion to methane in different pathways (Table 3). Compared with the mediated interspecies electron transfer (MIET) pathway, DIET pathway whereby acetate is oxidized to electrons and protons is thermodynamically more favourable since an energy benefit of 318.64 kJ/mol exists. The

Table 3
Reactions and changes in Gibbs free energy ($\Delta G^{0'}$) values of acetate conversion to methane in different pathways.

Process	Reaction	$\Delta G^{0'}$ (kJ/mol) [a]
Acetate oxidation	MIET: $CH_3COO^- + H^+ + 2H_2O \rightarrow 4H_2 + 2CO_2$	+94.78
	DIET: $CH_3COO^- + H^+ + 2H_2O \rightarrow 8H^+ + 8e^- + 2CO_2$	−223.86
Methanogenesis	MIET: $4H_2 + CO_2 \rightarrow CH_4 + 2H_2O$	−130.69
	DIET: $8H^+ + 8e^- + CO_2 \rightarrow CH_4 + 2H_2O$	+187.95
Overall	$CH_3COO^- + H^+ \rightarrow CH_4 + CO_2$	−35.91

[a] Values are calculated under the conditions of T = 298.15 K, pH = 7, Pressure = 1 atm, and [Reactants] = 1 M based on tabulated data by Ref. [54]; MIET: mediated interspecies electron transfer; DIET: direct interspecies electron transfer.

generated electrons can be directly utilized by some methanogens to produce methane [50]. However, this DIET strategy needs well-established connections between syntrophic acetogens and methanogens [4]. Graphene has been proven to act as an electron conduit to connect microbial populations and thereby enhance the DIET mechanism in AD systems due to its intrinsic properties of high electrical conductivity and enhanced biocompatibility [24,51,52]. The critical role of electrical conductivity in triggering DIET has been widely emphasized by other studies [19,50]. Compared with the control group, graphene amendment significantly enhanced the electrical conductivity of the biomethanation system. The electrical conductivity of the anaerobic sludge in the graphene amended group was 36.83 μS/cm, which is 264% higher than that of the control group (Table S1). Members of the genus *Methanothermobacter* have been reported to be actively involved in the DIET process with the supplementation of carbonaceous materials [50,53]. Compared with the control group, graphene addition led to the predominance of potential SAO OTUs in the order *SHA-98* and *Methanothermobacter*, which likely indicates enhanced connections between them *via* DIET and thereby facilitating resistance to the shock of intermittent gas supply.

The high specific surface area of graphene itself (500 m^2/g) may be another essential factor in stabilizing the biomethanation system. The high specific surface area of carbonaceous materials has been suggested to be responsible for improved methane production rate during *ex-situ* biomethanation [23]. This property has also been highlighted to enhance and stabilize the AD process [31,55]. Moreover, other physicochemical properties of carbonaceous materials such as hydrophobicity and surface functional groups have been suggested to positively influence the adhesion of microbes [56,57]. The enrichment of functional microbes tightly adhered to the carbonaceous materials due to its porous structure is suggested to be an efficient strategy to resist external stresses [22,58]. Based on the above discussion, the potential mechanism which explains the stabilization effect of graphene on *ex-situ* biomethanation is proposed and shown in Fig. 9. With the intermittent gas injection, graphene addition possibly led to the alteration of a metabolic pathway to a SAO process with the cooperation between possible SAO OTUs within the order *SHA-98* and methanogens within genus *Methanothermobacter*. The high electrical conductivity, large specific surface area and enhanced biocompatibility of graphene is postulated to play an essential role in influencing system performance with the shock of intermittent gas supply.

3.6. Practical implications of the present study

P2G based biomethanation technologies enable the production of biomethane utilising renewable H_2 from curtailed electricity and biogenic CO_2 from biogas. It is estimated that approximately 13.5 billion m^3 CO_2 from existing biogas and biomethane plants in Europe could be methanised in 2018 [59]. Meanwhile, global renewables are expected to overtake fossil fuels (such as coal) as the leading source of electricity generation by 2025 [60]. This indicates the considerable potential and resource for P2G technologies. Moreover, techno-economic analyses have been conducted in the literature to assess the sustainability of P2G systems in different scenarios. For example, Truc et al. [61] investigated the sustainability of P2G systems using CO_2 from biogas and H_2 from renewable electricity to produce methane; results revealed that this system is more sustainable than traditional upgrading technology (such as amine scrubber) if the renewable electricity is significantly decarbonised. However, the intermittency in renewable hydrogen availability associated with intermittency in production of green electricity may add a technical challenge to the optimal operation of the biomethanation system, thereby affecting its biological sustainability.

The present work pioneers an innovative solution to achieve efficient and robust biogas upgrading performance by combining carbonaceous material amendment with P2G based biomethanation. Nanomaterial graphene and the more cost-effective pyrochar were used as representative carbonaceous materials to enhance the robustness of the biomethanation process. A major finding from this study reveals that graphene addition can improve the gas conversion efficiency by 18.2% and the production rate by 267% compared with that of the control after repetitive intermittent supply of hydrogen generating a repetitive stop-go operation of the system. This finding may conceivably extend to other biomethanation systems, in which different reactor configurations are used [14]. Notably, some data points obtained at the end of each cycle have high standard deviations, which might affect the reliability of the findings. However, the dynamic upgrading profile clearly showed that graphene amendment induced a significant stabilization effect on *ex-situ* biomethanation. One drawback may be related to the high price of graphene (typical price €644/kg in the form of nanosheets [18]), which may hinder its practical application on an industrial scale. Unlike the conventional addition-reaction-discharge strategy for additives in biological conversion technologies (such as fermentation and AD), the introduced carbonaceous materials in biomethanation systems can be retained within the reactor during upgrading since the input and output products are both gaseous; this can reduce the economic penalty of using expensive graphene. This is the rationale for assessing pyrochar, which is much cheaper (average price €3/kg [18]) than graphene, and as such should lead to cost reductions. Dedicated experiments on optimising pyrochar dosages and properties are necessary to maximize the potential stabilization effects on biomethanation caused by intermittency of operation. To further understand the efficacy of the system within the biofuel industry it is necessary to evaluate the sustainability of the entire system [62]. Evidence based scientific literature is needed to assess economic and environmental sustainability of the biomethanation system integrated with carbonaceous material amendment. In line with this, exergy-based methods enabling the combination of thermodynamic, economic and environmental assessments may be the most relevant tool for such an assessment [63].

4. Conclusions and future directions

This study demonstrated that graphene amendment can help stabilize *ex-situ* biomethanation after experiencing intermittent gas supply, possibly due to the high electrical conductivity and large specific surface

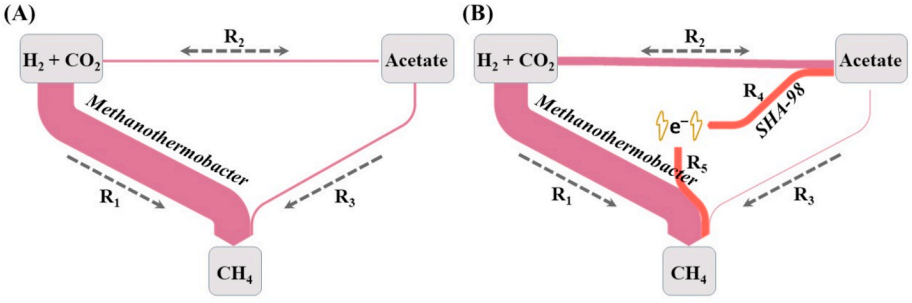


Fig. 9. Potential reactions involved in the control group (A) and graphene group (B) with intermittent gas injection (R_1: hydrogenotrophic methanogenesis ($4H_2 + CO_2 \rightarrow CH_4 + 2H_2O$); R_2: homoacetogenesis and acetogenesis ($4H_2 + 2CO_2 \leftrightarrow CH_3COO^- + H^+ + 2H_2O$); R_3: acetoclastic methanogenesis ($CH_3COO^- + H^+ \rightarrow CH_4 + CO_2$); R_4: acetate oxidation *via* direct interspecies electron transfer ($CH_3COO^- + H^+ + 2H_2O \rightarrow 8H^+ + 8e^- + 2CO_2$); R_5: methanogenesis *via* direct interspecies electron transfer ($8H^+ + 8e^- + CO_2 \rightarrow CH_4 + 2H_2O$)).

area of graphene. With the shock of intermittent gas injection, graphene addition enhanced the gas conversion efficiency by 18.2% and production rate by 267% as compared with the control. However, pyrochar amendment did not lead to promotional effects on the upgrading performance. Microbial analysis showed that OTUs belonging to the order *SHA-98* induced by graphene addition and archaea from the genus *Methanothermobacter* potentially altered the metabolic pathway to a syntrophic acetate oxidation process to stabilize the upgrading performance.

For future research, the use of in depth molecular microbial analysis involving both metagenomics and transcriptomics will be necessary to shed further light on the functional microorganisms involved in stabilizing biomethanation systems resulting from graphene amendment. Intermediate product analysis is also needed to further investigate the potential mechanism. For pyrochar addition, the low dosage and surface area of the pyrochar used in this study are assumed to be ascribed to the poor enhancing effects on biomethanation. Further study is required to investigate the potential correlation between the properties of pyrochar (such as surface functional group, specific surface area, and dosage) and the effect on upgrading performance with repetitive intermittent gas injection. This study was performed in a semi-batch mode to assess the efficacy of the hypothesis that carbonaceous materials could enhance the robustness of *ex-situ* biomethanation systems. With the results obtained under the batch mode, continuous reactor trials are needed to investigate the potential effect of carbonaceous materials on the *ex-situ* biomethanation process. Another important research focus would be an evaluation of the sustainability of the carbonaceous materials-amended biomethanation system using appropriate assessment tools such as exergy-based analyses.

Declaration of competing interest

The authors declare that they have no known competing financial interests or personal relationships that could have appeared to influence the work reported in this paper.

Acknowledgements

This work is funded under the Ireland Environmental Protection Agency (EPA) Research Programme 2014–2020 (No. 2018-RE-MS-13), Science Foundation Ireland (SFI) through the MaREI Centre for Energy, Climate and Marine under grant No. 12/RC/2302_P2 and 16/SP/3829, and Sustainable Energy Authority Ireland (No. RDD/00454). The EPA Research Programme is a Government of Ireland initiative funded by the Department of Communications, Climate Action and Environment.

Appendix A. Supplementary data

Supplementary data to this article can be found online at https://doi.org/10.1016/j.rser.2021.111690.

Credit author statement

Benteng Wu: Conceptualization; Methodology; Investigation; Writing – original draft. Richen Lin: Conceptualization, Methodology; Supervision; Validation; Funding acquisition; Writing – review & editing. Xihui Kang: Investigation; Writing – review & editing. Chen Deng: Investigation; Writing – review & editing. Alan D.W. Dobson: Validation; Writing – review & editing. Jerry D Murphy: Conceptualization; Validation; Project administration; Supervision; Funding acquisition; Writing – review & editing.

References

[1] Salimijazi F, Kim J, Schmitz AM, Grenville R, Bocarsly A, Barstow B. Constraints on the efficiency of engineered electromicrobial production. Joule 2020;4:2101–30.
[2] Strübing D, Moeller AB, Mößnang B, Lebuhn M, Drewes JE, Koch K. Anaerobic thermophilic trickle bed reactor as a promising technology for flexible and demand-oriented H_2/CO_2 biomethanation. Appl Energy 2018;232:543–54.
[3] del Pilar Anzola Rojas M, Mateos R, Sotres A, Zaiat M, Gonzalez ER, Escapa A, et al. Microbial electrosynthesis (MES) from CO_2 is resilient to fluctuations in renewable energy supply. Energy Convers Manag 2018;177:272–9.
[4] Wu B, Lin R, O'Shea R, Deng C, Rajendran K, Murphy JD. Production of advanced fuels through integration of biological, thermo-chemical and power to gas technologies in a circular cascading bio-based system. Renew Sustain Energy Rev 2021;135:110371.
[5] Lin R, Deng C, Zhang W, Hollmann F, Murphy JD. Production of bio-alkanes from biomass and CO_2. Trends Biotechnol 2021;39:370–80.
[6] Logroño W, Popp D, Nikolausz M, Kluge P, Harms H, Kleinsteuber S. Microbial communities in flexible biomethanation of hydrogen are functionally resilient upon starvation. Front Microbiol 2021:12.
[7] Persson T, MurPhy J, Jannasch A-K, Ahern E, Liebetrau J, Trommler M, et al. A perspective on the potential role of biogas in smart energy grids. IEA Bioenergy Paris; 2014.
[8] Gnanakumar ES, Chandran N, Kozhevnikov IV, Grau-Atienza A, Ramos Fernández EV, Sepulveda-Escribano A, et al. Highly efficient nickel-niobia composite catalysts for hydrogenation of CO_2 to methane. Chem Eng Sci 2019;194:2–9.
[9] Omar B, El-Gammal M, Abou-Shanab R, Fotidis IA, Angelidaki I, Zhang Y. Biogas upgrading and biochemical production from gas fermentation: impact of microbial community and gas composition. Bioresour Technol 2019;286:121413.
[10] Guneratnam AJ, Ahern E, FitzGerald JA, Jackson SA, Xia A, Dobson ADW, et al. Study of the performance of a thermophilic biological methanation system. Bioresour Technol 2017;225:308–15.
[11] Fu S, Angelidaki I, Zhang Y. *In situ* biogas upgrading by CO_2-to-CH_4 bioconversion. Trends Biotechnol 2021;39:336–47.
[12] Bassani I, Kougias PG, Treu L, Angelidaki I. Biogas upgrading *via* hydrogenotrophic methanogenesis in two-stage continuous stirred tank reactors at mesophilic and thermophilic conditions. Environ Sci Technol 2015;49:12585–93.
[13] Voelklein MA, Rusmanis D, Murphy JD. Biological methanation: strategies for *in-situ* and *ex-situ* upgrading in anaerobic digestion. Appl Energy 2019;235:1061–71.
[14] Kougias PG, Treu L, Benavente DP, Boe K, Campanaro S, Angelidaki I. *Ex-situ* biogas upgrading and enhancement in different reactor systems. Bioresour Technol 2017;225:429–37.
[15] Rachbauer L, Voitl G, Bochmann G, Fuchs W. Biological biogas upgrading capacity of a hydrogenotrophic community in a trickle-bed reactor. Appl Energy 2016;180:483–90.
[16] McDonagh S, Deane P, Rajendran K, Murphy JD. Are electrofuels a sustainable transport fuel? Analysis of the effect of controls on carbon, curtailment, and cost of hydrogen. Appl Energy 2019;247:716–30.
[17] Wu B, Lin R, Kang X, Deng C, Xia A, Dobson ADW, et al. Graphene addition to digestion of thin stillage can alleviate acidic shock and improve biomethane production. ACS Sustainable Chem Eng 2020;8:13248–60.
[18] Deng C, Lin R, Kang X, Wu B, O'Shea R, Murphy JD. Improving gaseous biofuel yield from seaweed through a cascading circular bioenergy system integrating anaerobic digestion and pyrolysis. Renew Sustain Energy Rev 2020;128:109895.
[19] Tan LC, Lin R, Murphy JD, Lens PNL. Granular activated carbon supplementation enhances anaerobic digestion of lipid-rich wastewaters. Renew Energy 2021.
[20] Nizami A-S, Rehan M. Towards nanotechnology-based biofuel industry. Biofuel Res J 2018;5:798–9.
[21] Dehhaghi M, Tabatabaei M, Aghbashlo M, Kazemi Shariat Panahi H, Nizami A-S. A state-of-the-art review on the application of nanomaterials for enhancing biogas production. J Environ Manag 2019;251:109597.
[22] Lü F, Luo C, Shao L, He P. Biochar alleviates combined stress of ammonium and acids by firstly enriching *Methanosaeta* and then *Methanosarcina*. Water Res 2016;90:34–43.
[23] Yang H-J, Yang Z-M, Xu X-H, Guo R-B. Increasing the methane production rate of hydrogenotrophic methanogens using biochar as a biocarrier. Bioresour Technol 2020;302:122829.
[24] Lin R, Deng C, Cheng J, Xia A, Lens PNL, Jackson SA, et al. Graphene facilitates biomethane production from protein-derived glycine in anaerobic digestion. iScience 2018;10:158–70.
[25] Zhao Z, Zhang Y, Yu Q, Dang Y, Li Y, Quan X. Communities stimulated with ethanol to perform direct interspecies electron transfer for syntrophic metabolism of propionate and butyrate. Water Res 2016;102:475–84.
[26] Tsapekos P, Treu L, Campanaro S, Centurion VB, Zhu X, Peprah M, et al. Pilot-scale biomethanation in a trickle bed reactor: process performance and microbiome functional reconstruction. Energy Convers Manag 2021;244:114491.
[27] Lin R, Cheng J, Zhang J, Zhou J, Cen K, Murphy JD. Boosting biomethane yield and production rate with graphene: the potential of direct interspecies electron transfer in anaerobic digestion. Bioresour Technol 2017;239:345–52.
[28] Shen Y, Linville JL, Urgun-Demirtas M, Schoene RP, Snyder SW. Producing pipeline-quality biomethane *via* anaerobic digestion of sludge amended with corn stover biochar with *in-situ* CO_2 removal. Appl Energy 2015;158:300–9.
[29] Linville JL, Shen Y, Ignacio-de Leon PA, Schoene RP, Urgun-Demirtas M. *In-situ* biogas upgrading during anaerobic digestion of food waste amended with walnut shell biochar at bench scale. Waste Manag Res 2017;35:669–79.
[30] Li D, Song L, Fang H, Li P, Teng Y, Li Y-Y, et al. Accelerated bio-methane production rate in thermophilic digestion of cardboard with appropriate biochar: dose-response kinetic assays, hybrid synergistic mechanism, and microbial networks analysis. Bioresour Technol 2019;290:121782.

[31] Lü F, Liu Y, Shao L, He P. Powdered biochar doubled microbial growth in anaerobic digestion of oil. Appl Energy 2019;247:605–14.
[32] Jensen MB, Strübing D, de Jonge N, Nielsen JL, Ottosen LDM, Koch K, et al. Stick or leave – pushing methanogens to biofilm formation for *ex situ* biomethanation. Bioresour Technol 2019;291:121784.
[33] Rachbauer L, Beyer R, Bochmann G, Fuchs W. Characteristics of adapted hydrogenotrophic community during biomethanation. Sci Total Environ 2017;595:912–9.
[34] Zhou H, Xing D, Xu M, Su Y, Zhang Y. Biogas upgrading and energy storage *via* electromethanogenesis using intact anaerobic granular sludge as biocathode. Appl Energy 2020;269:115101.
[35] de Jonge N, Moset V, Møller HB, Nielsen JL. Microbial population dynamics in continuous anaerobic digester systems during start up, stable conditions and recovery after starvation. Bioresour Technol 2017;232:313–20.
[36] Zhao Z, Zhang Y, Li Y, Dang Y, Zhu T, Quan X. Potentially shifting from interspecies hydrogen transfer to direct interspecies electron transfer for syntrophic metabolism to resist acidic impact with conductive carbon cloth. Chem Eng J 2017;313:10–8.
[37] Wang C, Liu Y, Jin S, Chen H, Xu X, Wang Z, et al. Responsiveness extracellular electron transfer (EET) enhancement of anaerobic digestion system during start-up and starvation recovery stages *via* magnetite addition. Bioresour Technol 2019;272:162–70.
[38] Zheng Z, Cai Y, Zhang Y, Zhao Y, Gao Y, Cui Z, et al. The effects of C/N (10–25) on the relationship of substrates, metabolites, and microorganisms in "inhibited steady-state" of anaerobic digestion. Water Res 2021;188:116466.
[39] Chen Y-T, Zeng Y, Li J, Zhao X-Y, Yi Y, Gou M, et al. Novel syntrophic isovalerate-degrading bacteria and their energetic cooperation with methanogens in methanogenic chemostats. Environ Sci Technol 2020;54:9618–28.
[40] Jackson SA, Kang X, O'Shea R, O'Leary N, Murphy JD, Dobson ADW. Anaerobic digestion performance and microbial community structures in biogas production from whiskey distillers organic by-products. Bioresour Technol Rep 2020;12:100565.
[41] Zamanzadeh M, Hagen LH, Svensson K, Linjordet R, Horn SJ. Anaerobic digestion of food waste – effect of recirculation and temperature on performance and microbiology. Water Res 2016;96:246–54.
[42] Tian H, Mancini E, Treu L, Angelidaki I, Fotidis IA. Bioaugmentation strategy for overcoming ammonia inhibition during biomethanation of a protein-rich substrate. Chemosphere 2019;231:415–22.
[43] Müller B, Sun L, Westerholm M, Schnürer A. Bacterial community composition and fhs profiles of low- and high-ammonia biogas digesters reveal novel syntrophic acetate-oxidising bacteria. Biotechnol Biofuels 2016;9:48.
[44] Bassani I, Kougias PG, Treu L, Porté H, Campanaro S, Angelidaki I. Optimization of hydrogen dispersion in thermophilic up-flow reactors for *ex situ* biogas upgrading. Bioresour Technol 2017;234:310–9.
[45] Wu B, He C, Yuan S, Hu Z, Wang W. Hydrogen enrichment as a bioaugmentation tool to alleviate ammonia inhibition on anaerobic digestion of phenol-containing wastewater. Bioresour Technol 2019;276:97–102.
[46] Wintsche B, Jehmlich N, Popp D, Harms H, Kleinsteuber S. Metabolic adaptation of methanogens in anaerobic digesters upon trace element limitation. Front Microbiol 2018;9.
[47] Kougias PG, Tsapekos P, Treu L, Kostoula M, Campanaro S, Lyberatos G, et al. Biological CO_2 fixation in up-flow reactors *via* exogenous H_2 addition. J Biotechnol 2020;319:1–7.
[48] Prathiviraj R, Chellapandi P. Comparative genomic analysis reveals starvation survival systems in *Methanothermobacter thermautotrophicus* ΔH. Anaerobe 2020;64:102216.
[49] De Vrieze J, Hennebel T, Boon N, Verstraete W. *Methanosarcina*: the rediscovered methanogen for heavy duty biomethanation. Bioresour Technol 2012;112:1–9.
[50] Zhao Z, Li Y, Zhang Y, Lovley DR. Sparking anaerobic digestion: promoting direct interspecies electron transfer to enhance methane production. iScience 2020;23:101794.
[51] Wu Z-S, Ren W, Gao L, Zhao J, Chen Z, Liu B, et al. Synthesis of graphene sheets with high electrical conductivity and good thermal stability by hydrogen arc discharge exfoliation. ACS Nano 2009;3:411–7.
[52] Lin R, Cheng J, Ding L, Murphy JD. Improved efficiency of anaerobic digestion through direct interspecies electron transfer at mesophilic and thermophilic temperature ranges. Chem Eng J 2018;350:681–91.
[53] Yin C, Shen Y, Yuan R, Zhu N, Yuan H, Lou Z. Sludge-based biochar-assisted thermophilic anaerobic digestion of waste-activated sludge in microbial electrolysis cell for methane production. Bioresour Technol 2019;284:315–24.
[54] Madigan MT, Martinko JM, Bender KS, Buckley DH, Stahl DA. Brock biology of microorganisms. 14 ed. Pearson Education; 2014.
[55] Dang Y, Sun D, Woodard TL, Wang L-Y, Nevin KP, Holmes DE. Stimulation of the anaerobic digestion of the dry organic fraction of municipal solid waste (OFMSW) with carbon-based conductive materials. Bioresour Technol 2017;238:30–8.
[56] Umetsu M, Sunouchi T, Fukuda Y, Takahashi H, Tada C. Functional group distribution of the carrier surface influences adhesion of *Methanothermobacter thermautotrophicus*. Archaea 2020;2020:9432803.
[57] Habouzit F, Gévaudan G, Hamelin J, Steyer J-P, Bernet N. Influence of support material properties on the potential selection of *Archaea* during initial adhesion of a methanogenic consortium. Bioresour Technol 2011;102:4054–60.
[58] Luo C, Lü F, Shao L, He P. Application of eco-compatible biochar in anaerobic digestion to relieve acid stress and promote the selective colonization of functional microbes. Water Res 2015;68:710–8.
[59] European Biogas Association. Annual Statistical Report. 2018. https://www.europeanbiogas.eu/wp-content/uploads/2019/05/EBA_Statistical-Report-2018_Abriged Public_web.pdf. [Accessed 13 July 2020]. EBA 2018.
[60] International Energy Agency. Renewables 2020, paris. 2020. https://www.iea.org/reports/renewables-2020. [Accessed 13 July 2021]. IEA.
[61] Vo TTQ, Wall DM, Ring D, Rajendran K, Murphy JD. Techno-economic analysis of biogas upgrading *via* amine scrubber, carbon capture and *ex-situ* methanation. Appl Energy 2018;212:1191–202.
[62] Rosen MA. Environmental sustainability tools in the biofuel industry. Biofuel Res J 2018;5:751–2.
[63] Aghbashlo M, Tabatabaei M, Soltanian S, Ghanavati H. Biopower and biofertilizer production from organic municipal solid waste: an exergoenvironmental analysis. Renew Energy 2019;143:64–76.